Int. J. Multiphase Flow Vol. 13, No. 5, pp. 671–684, 1987
Printed in Great Britain.
0301-9322/87 $3.00 + 0.00

NUMERICAL SIMULATION OF GAS–SOLID TWO-PHASE FLOW IN A TWO-DIMENSIONAL HORIZONTAL CHANNEL

Y. TSUJI, Y. MORIKAWA, T. TANAKA, N. NAKATSUKASA and M. NAKATANI
Faculty of Engineering, Osaka University, Suita, Osaka 565, Japan

(*Received* 1 *August* 1986; *in revised form* 17 *March* 1987)

Abstract—A numerical simulation was made to determine the motion of particles and fluid in a horizontal channel. The simulation was based on the Lagrangian method for the solid phase, where trajectories of many particles are calculated by integrating the equations of motion of a single particle. The fluid motion was solved using a finite-difference method simultaneously with the particle motion. The present simulation requires some empirical parameters concerning the collision of the particles with the wall. These parameters were determined by comparisons between calculated results and measurements.

1. INTRODUCTION

Research workers in the field of multiphase flows are stimulated by the high potential of numerical fluid-mechanics for single-phase flows and thus take note of the simulation of flows of interest. In fact, several recently published works report on gas–solid flows, especially free-jets (Shuen *et al.* 1985; Mostafa & Elghobashi 1985; Chen & Wood 1986). However, the same simulation procedure as in wall-free flows cannot always be applied to the corresponding pipe flows, because particles collide frequently with the pipe wall, resulting in additional losses of kinetic energy. One of the most important factors in dealing with collisions is that collisions accompany irregularity. This irregularity plays an important role as the necessary mechanism by which particles are conveyed in a horizontal pipe. Hence, much effort has been directed towards the problem of particle–wall collisions (Matsumoto *et al.* 1976; Tsuji & Morikawa 1978; Tsuji *et al.* 1983, 1985). However, our approach has had the following problem.

We used the Lagrangian method to obtain the motion of the solid phase, and assumed that the fluid phase is not affected locally by the presence of particles except for the additional loss of pressure. Trajectories of individual particles were calculated in a flow field given beforehand by integrating the equations of motion and assuming the coefficient of restitution and kinetic friction. As a result, the behavior of particles in the pipe and the pressure drop could be predicted satisfactorily to some extent. However, it is well-known that fluid velocity profiles are distorted by particles, even at a low volume concentration, if the number concentration is high. Therefore, improvement of our simulation model was required so that the fluid velocity profiles could be calculated. Such a simulation, taking into account the interaction between local fluid velocity and particle motion, has already been attempted by Durst *et al.* (1984) for vertical pipe flow, though they ignored particle–wall collisions.

We considered a horizontal flow in this work, where asymmetric behavior due to gravity is clearly observed, and we analyzed a two-dimensional channel flow as the first stage in our attempt. The Lagrangian method was adopted here also to calculate the solid phase. For the calculation of the fluid phase, the method developed by Patankar & Spalding (1970) was used in combination with the PSI-Cell model (Crowe *et al.* 1977), which is necessary for taking into account the interaction between the solid and fluid phases. Regarding the collision between particles and the wall, "the virtual wall model" was used in addition to the ordinary relation of the collision between spherical particles and a wall. Tsuji *et al.* (1985) proposed this model to enable spherical particles to continue to bounce on the horizontal wall under the influence of gravity. Unfortunately, since an exact solution of irregular collisions for arbitrary shaped materials is difficult at the moment, one cannot help depending on an empirical method, where several unknown parameters need be determined empirically. Therefore, an experimental transport facility with a horizontal channel was

constructed for comparisons between calculated and experimental results. In the course of this work, a defect in the previous bouncing model was found and modified by referring to measurements. The present simulation results were compared with experimental ones with regard to the particle and fluid velocity distributions, particle concentrations and pressure drops.

2. BASIC EQUATIONS

2.1. Equation of Fluid Motion

Fluid motion between two parallel plates, shown in figure 1, is given by the boundary layer equation

$$\rho u \frac{\partial u}{\partial x} = \frac{\partial \tau}{\partial \psi} - \frac{\mathrm{d}p}{\mathrm{d}x} - f_\mathrm{p}, \qquad [1]$$

where

u = the time-averaged fluid velocity,
τ = shear stress,
p = pressure,
f_p = force exerted by the particles on a unit volume of fluid.

Following Patankar & Spalding (1970), the dimensionless stream function ω is introduced:

$$\omega = \frac{\psi}{\psi_0}, \qquad [2]$$

where ψ and ψ_0 are defined by

$$\frac{\partial \psi}{\partial y} = \rho u \qquad [3]$$

and

$$\psi_0 = \int_0^h \rho u \, \mathrm{d}y. \qquad [4]$$

Using the (x, ω) system instead of (x, ψ) coordinates and rewriting [1]:

$$\frac{\partial u}{\partial x} = \frac{1}{\psi_0}\frac{\partial \tau}{\partial \omega} - \frac{1}{\rho u}\left(-\frac{\mathrm{d}p}{\mathrm{d}x} - f_\mathrm{p}\right). \qquad [5]$$

Since the above equation is a boundary layer type, the finite-difference form of it can be solved from the upstream side by turns using the so-called marching method which does not require repetition. In the present calculation, the flow field was divided into 14 segments in the y-direction and the marching step in the x-direction was set to be half the channel height.

The effects of particles on the fluid velocity can be taken into account through the term f_p in [1] and [5], because this term shows the momentum exchange between the fluid and solid phases. The definite expression of f_p is deduced from the differences in momentum of the particles between the instant of entering and on leaving the control volume. That is, the term f_p is expressed as

$$f_\mathrm{p} = \frac{nm}{\Delta V_i} \cdot \frac{\Delta v_\mathrm{s}}{\Delta t} \qquad [6]$$

when the particles exist within the region (volume $= \Delta V_i$) shown by the dotted line in figure 2, where n = the number of particles in the region, m = the mass of a principle, Δv_s = the difference in particle velocity between the two instants when the particle enters the control volume and leaves

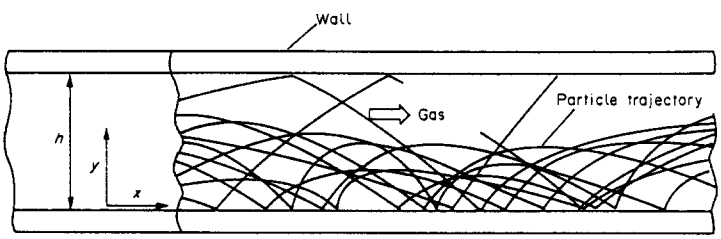

Figure 1. Gas–solid two-phase flow in a horizontal channel.

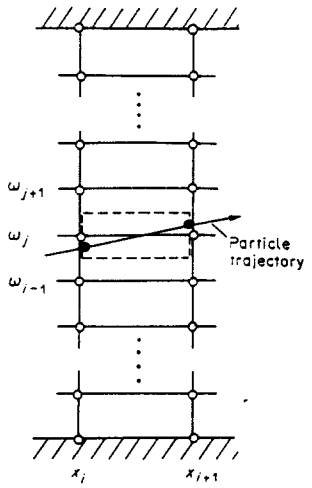

Figure 2. Grid and control volume.

it and Δt = the time for which the particle remains in the region. If all the particles follow the same trajectory, the number n corresponding to the control volume considered is given by

$$n = \frac{q\Delta t}{m}, \qquad [7]$$

where q denotes the particle mass flow rate. Substituting [7] into [6], one obtains

$$f_p = \frac{q\Delta v_s}{\Delta V_i}. \qquad [8]$$

If one assumes that all the particles follows the same line, it would be sufficient to obtain a trajectory for only one particle. This assumption means that no particles exist in other regions. In practice however, needless to say, many particles exist in many control volumes at the same time. Therefore, we use the following method.

First, calculations of trajectory are made for many particles with different initial conditions, and the trajectory of each particle is recorded. The term f_p is calculated for each particle and each control volume using [8]. The values of f_p are then divided by the number of particles, which is equal to the number of calculation trials. If these values are given to the regions through which the particles pass, it leads to the equivalent result for when many particles are simultaneously in many regions.

2.2. Equations of Eddy Viscosity and Pressure Loss

There are several models of eddy viscosity available which consider the effect of particles. However they are for the case of fine particles, and thus we neglect such an effect in the present simulation as our first approximation.

Regarding the shear stress, the following expression is adopted:

$$\tau = \rho(\nu + \nu_{\text{eff}})\frac{\partial u}{\partial y}; \qquad [9]$$

and mixing length theory is applied to the kinematic eddy viscosity ν_{eff} in the same way as in single-phase flows.

For the pressure gradient along the flow, the equation

$$\frac{dp}{dx} = -\frac{\tau_u + \tau_l}{h} - \bar{f}_p \qquad [10]$$

is used, where τ_u and τ_l are the shear stresses on the upper and lower walls, respectively, and $\bar{f}_p$ is the value of f_p averaged over the cross section. Equation [10] is derived from the one-dimensional conservation law of momentum.

2.3. Equation of Particle Motion

Particle motion is given by the following equation:

$$\frac{\mathrm{d}}{\mathrm{d}t}\begin{bmatrix} v_x \\ v_y \end{bmatrix} = \frac{3}{4}\frac{\rho(\mathbf{u}-\mathbf{v})}{(\rho_p + \frac{1}{2}\rho)\, d_p}\left\{ C_D \begin{bmatrix} u - v_x \\ -v_y \end{bmatrix} + C_{Lr}\begin{bmatrix} -v_y \\ -u + v_x \end{bmatrix}\right\}$$

$$+ C_{Ls}\frac{1}{(\rho_p + \frac{1}{2}\rho)V_p}\begin{bmatrix} v_y \dfrac{\partial u}{\partial y} \\ (u - v_x)\dfrac{\partial u}{\partial y} \end{bmatrix} + \frac{\rho_p - \rho}{\rho_p + \frac{1}{2}\rho}\begin{bmatrix} 0 \\ -g \end{bmatrix}, \quad [11]$$

where

$\mathbf{v}, \mathbf{u}$ = vectors of particle and fluid velocity vectors, respectively,
v_x, v_y = x-, y-components of particle velocity,
d_p = particle diameter,
ρ_p, ρ = particle and fluid density, respectively,
V_p = volume of one particle,
C_D = drag coefficient,
C_{Lr}, C_{Ls} = coefficients of life due to particle rotation and velocity shear, respectively.

In order to obtain the particle motion using [11], the cofficients C_D, C_{Lr} and C_{Ls} must be known. Fortunately, existing formula are available for the coefficients C_D and C_{Lr} in the same range of Reynolds number as in the present flow. For the coefficient C_{Ls}, the theoretical result by Saffman (1965) was used at first, although it is a solution for low Reynolds numbers. However, the lift force due to shear was not taken into account in most calculations in this work, because its contribution to the resulting trajectory was found to be negligible. In addition to the drag and lift forces, we took the dissipation of particle rotation into account by using the result of Dennis *et al.* (1980).

The most difficult problem in calculating trajectories in pipes and ducts is the effect of particle collisions with the wall. When a spherical particle collides with a flat plate, as shown in figure 3, the relations between the velocities before and after the collision are obtained by the impulsive equations. The results are shown in table 1 (Tsuji *et al.* 1985). An explanation of the results in table 1 is given in the Appendix. If the spherical particles do not collide too frequently, these relations are sufficient to consider the effect of collisions—even in a horizontal channel. However, if a perfect sphere collides with a perfect plane wall with a coefficient of restitution <1, this results in all particles sliding along the bottom of the wall after a number of collisions. To avoid such deposition, a model is necessary, and in our previous work (Tsuji *et al.* 1985) we proposed the "abnormal bouncing model", which is described in detail below.

2.4. The Abnormal Bouncing Model

As described above, a mechanism of abnormal bouncing is necessary to enable spherical particles to continue to fly in a horizontal pipe or channel under the influence of gravity. The virtual wall model which we proposed is shown in figure 4. In this model, the actual wall is replaced by a virtual one with an inclined angle α, if the incident angle η of a particle against the wall is less than a certain specified value. In order to estimate the momentum loss due to the collision with the virtual wall, the relation shown in table 1 can be used. When the particle collides with this virtual wall, the momentum of the particle is transformed effectively into the momentum in the y-direction after the collision. Therefore the particle continues to bounce on the wall, even though the coefficient

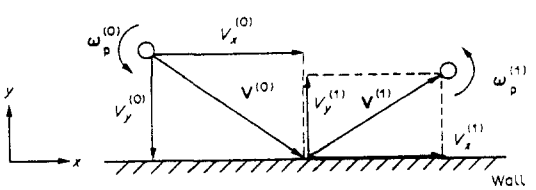

Figure 3. Collision between a particle and wall.

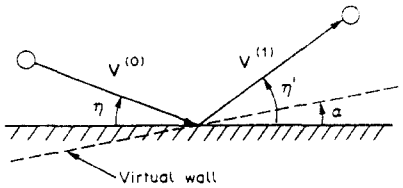

Figure 4. Virtual wall model.

Table 1. Solution of the impulsive equations

	Condition	Velocity	Angular velocity
(1)	$\frac{V_Y^{(0)}}{\lvert V\rvert} < \frac{-2}{7f(e+1)}$	$V_X = \frac{5}{7}\left(V_X^{(0)} - \frac{2a}{5}\omega_Z^{(0)}\right)$	$\omega_X = \frac{V_z}{a}$
		$V_Y = -eV_Y^{(0)}$	$\omega_Y = \omega_Y^{(0)}$
		$V_Z = \frac{5}{7}\left(V_Z^{(0)} + \frac{2a}{5}x^{(0)}\right)$	$\omega_Z = -\frac{V_X}{a}$
(2)	$\frac{-2}{7f(e+1)} < \frac{V_Y^{(0)}}{\lvert V\rvert} < 0$	$V_X = V_X^{(0)} + \epsilon_X f(e+1)V_Y^{(0)}$	$\omega_X = \omega_X^{(0)} - \frac{5}{2a}\epsilon_Z f(e+1)V_Y^{(0)}$
		$V_Y = -eV_Y^{(0)}$	$\omega_Y = \omega_Y^{(0)}$
		$V_Z = V_Z^{(0)} + \epsilon_Z f(e+1)V_Y^{(0)}$	$\omega_Z = \omega_Z^{(0)} + \frac{5}{2a}\epsilon_X f(e+1)v_Y^{(0)}$

$$\lvert V\rvert = \sqrt{(V_X^{(0)} + a\omega_Z^{(0)})^2 + (V_Z^{(0)} - a\omega_X^{(0)})^2}$$

$$\epsilon_X = (V_X^{(0)} + a\omega_Z^{(0)})/\lvert V\rvert, \quad \epsilon_Z = (V_Z^{(0)} - a\omega_X^{(0)})/\lvert V\rvert$$

Definitions: e = coefficient of restitution; f = coefficient of kinetic friction; V_X, V_Y, V_Z = translation velocity in the X-, Y-, Z-direction, respectively; X, Y = coordinate shown in figure 3 as normal to the X-, Y-direction, respectively; ω_X, ω_Y, ω_Z = angular velocity in the X-, Y-, Z-direction, respectively; superscript 0 = before collision.

of restitution is < 1. However, it is necessary to make an assumption for the angle α. Tsuji *et al.* (1985) assumed the following equation for α:

$$\alpha = -\delta(\eta - \beta) \quad (\tau \leqslant \beta)$$
$$\alpha = 0 \quad (\tau > \beta); \qquad [12]$$

δ and β were given empirically as follows:

$$\delta = \frac{2.3}{\mathrm{Fr}} - \frac{91}{\mathrm{Fr}^2} + \frac{1231}{\mathrm{Fr}^3}$$

$$\beta = 7^\circ, \qquad [13]$$

where Fr is the Froude number $= \bar{u}/\sqrt{gh}$. The above relations were obtained from comparisons between experiments and pipeflow simulations (Tsuji *et al.* 1985), but their applicability has not been sufficiently confirmed. Hence, in this work the relations are re-examined and modified.

3. EXPERIMENTAL FACILITIES

Figure 5 shows an experimental pipeline constructed for comparison with the present simulation. A two-dimensional channel made of acrylic plate comprises the test section, the inside height and width of which were $h = 25$ mm and $w = 200$ mm, respectively. A Pitot tube was used to measure air velocity, and an optical fiber probe developed by Morikawa *et al.* (1986) was used to measure particle velocity and number density. Figure 6 shows the principle of the present optical fiber probe. Figure 7 presents the velocity distribution of air in the spanwise direction obtained with single-phase flow at measuring point ⑧. This figure indicates that the flow can be regarded as approximately two-dimensional. Results obtained under two-phase conditions are presented in the next section together with the results of the simulation.

4. RESULTS

The conditions adopted for the simulation, which are the same as in the experiment, are as follows:

particle diameter $d_p = 1$ mm,
particle density $\rho_p = 1000$ kg/m^3,

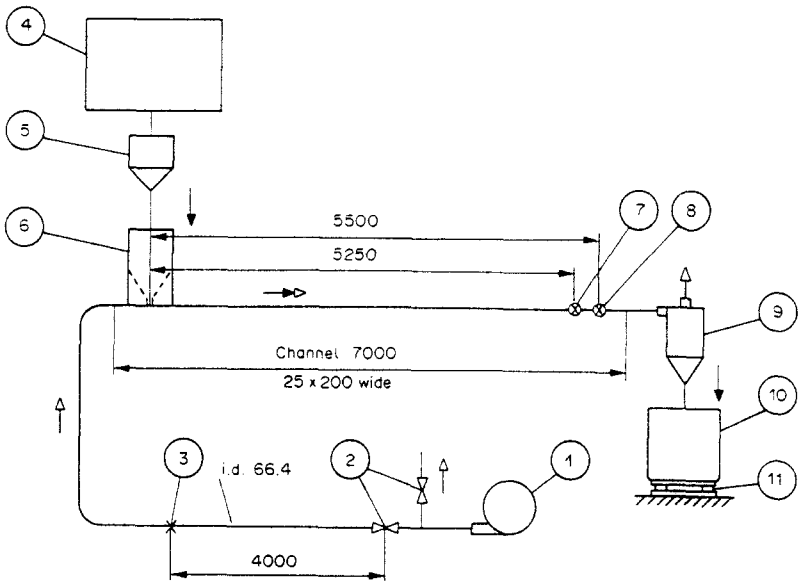

Figure 5. Experimental set up: ① blower, ② valve, ③ flow rate measuring section, ④ feed tank, ⑤ electromagnetic feeder, ⑥ particle disperser, ⑦ measuring section for particle velocity and concentration, ⑧ measuring section for air velocity, ⑨ cylone separator, ⑩ receiver tank, ⑪ load cell.

coefficient of restitution $e = 0.8$,
kinetic friction factor $f = 0.4$,
channel height $h = 25$ mm.

Standard air is assumed as the gas. In the experiment, polystyrene particles were used. It was assumed in the simulation that the particles are distributed uniformly in the initial section of the channel, $x = 0$, where particle velocities are half the mean air velocity $\bar{u}$ averaged over the cross section.

Particle trajectories without abnormal bouncing are shown in figure 8. In the figure, the scale of the longitudinal distance is greatly reduced so that the motion of the particles in the whole duct can be seen. It is seen in the figure that the vertical distance which particles reach in the channel decreases constantly due to collisions with the wall, because the coefficient of restitution is < 1. Resulting in all the particles sliding along the bottom of the wall in a region far from the initial point of calculation. The trajectories with abnormal bouncing are shown in figures 9a, b, where the two cases with and without the lift force due to shear are compared. Contrary to figure 8, the particles continue to repeat the bouncing motion, but the particle distribution is too close to the

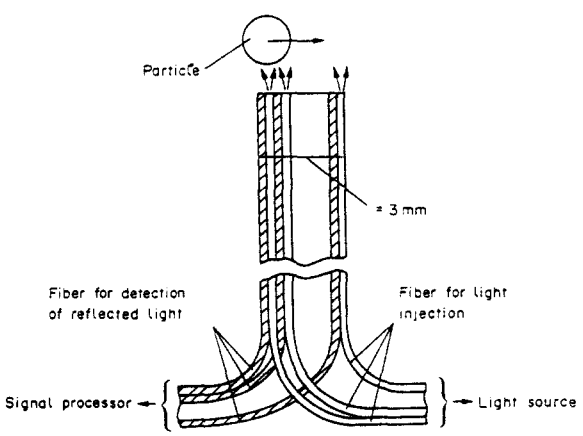

Figure 6. Optical fiber probe.

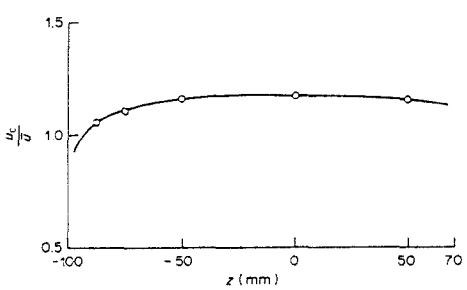

Figure 7. Velocity distribution of air in the spanwise direction (u_c = velocity at $y = h/2$, $\bar{u}$ = velocity averaged over the cross section).

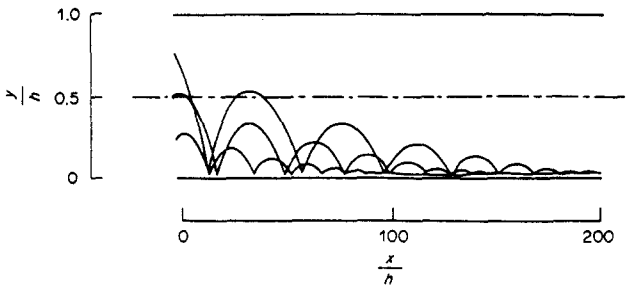

Figure 8. Particle trajectories without abnormal bouncing ($\bar{u}$ = 15 m/s).

bottom wall. It is found from comparison between figures 9a and 9b that the lift force definitely tends to lift the particles but, in general, its effect is small under the present conditions. Therefore, the lift due to shear was neglected in the later simulation.

One finds from the above results that the empirical relations [12] and [13] obtained for pipe flow cannot be applied directly to channel flow. The reason is as follows.

When dealing with abnormal bouncing in a pipe, irregularity in reflection in the z-direction was considered in addition to [12] and [13] so that the particles were dispersed not only in the r- and

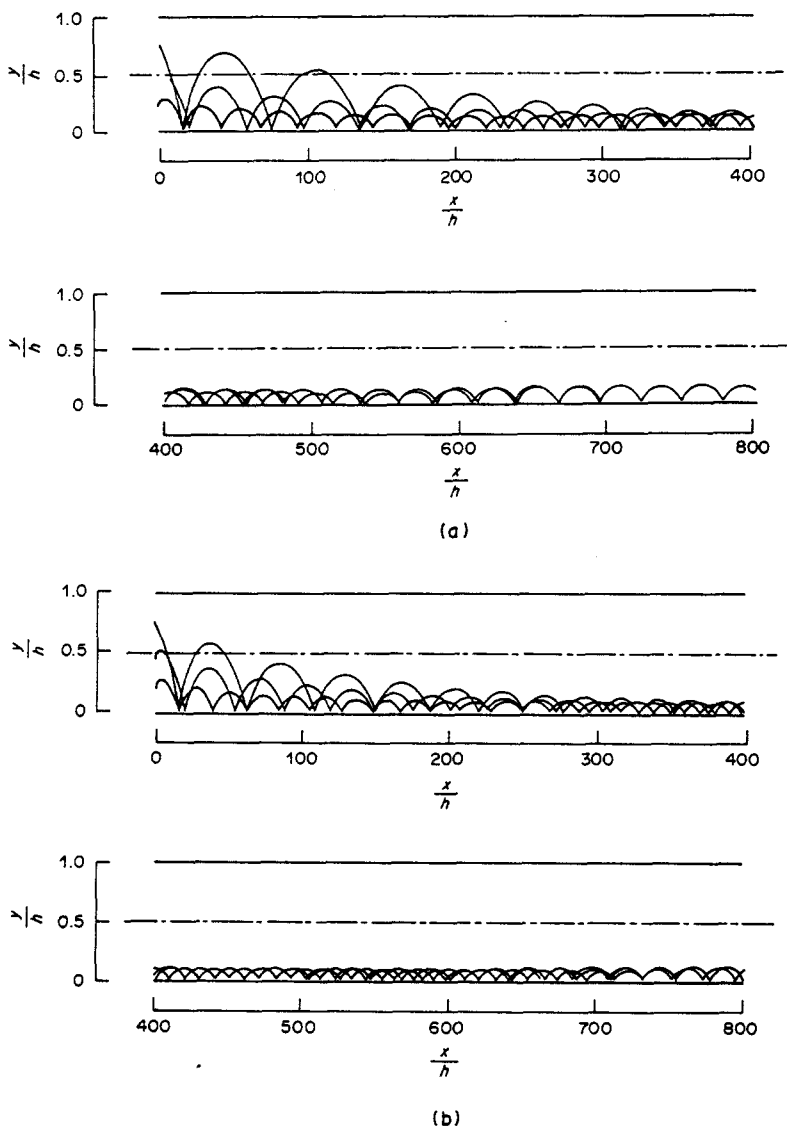

Figure 9. Particle trajectories ($\bar{u}$ = 15 m/s) (a) with lift force and (b) without lift force.

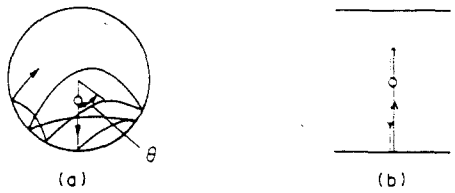

Figure 10. Bounce of a particle against a wall in (a) a pipe and (b) a two-dimensional channel.

z-directions but also in the θ-direction, as shown in figure 10. The angle of reflection in the θ-direction was termed the "yaw angle", which is given by random numbers. Consequently, some particles were lifted to a higher position due to collision with the wall and thus the particles were disperped widely in the pipe cross section. In the case of two-dimensional flow, the bouncing motion takes place only in the x- and y-directions. Therefore, so long as only [12] and [13] are used, the particle distribution does not become a realistic one.

The next stage in the present work is to improve the equations of the bouncing model by referring to the actual phenomena in the channel constructed for this purpose. As expected, an increase in the value of the coefficient δ in [12] makes the particles jump to a higher position after collision. For example, the particle trajectories shown in figure 11 are for a coefficient δ value three times as large as the one (δ_0) given by [12], i.e. $\delta = 3\delta_0$. In an experiment under the same conditions as in figure 11, we observed some particles colliding with the upper wall, though very few in number. However, figure 11 indicates that all particles show a similar pattern of trajectory and no particle collides with the upper wall. If a larger value is given to δ to make the particles collide with the upper wall, this results in all particles colliding with the wall. This means that an irregularity is necessary for the abnormal bouncing model of two-dimensional flow also, in order to simulate particle motion. In pipe flows, random numbers for the yaw angle cause such an irregularity. Hence, it was attempted here to multiply the coefficient δ by a random number R. First, the coefficient is expressed as

$$\delta = 5R\delta_0, \qquad [14]$$

and the corresponding trajectories are shown in figure 12. The calculation appears to give good results but on observing the figure more closely, one notices that the particle concentration is not higher near the lower wall. This is not true in actual horizontal flows. However, as long as [14] is used, the concentration has a maximum value near the center of the duct and remains low near the lower wall, even at a low air velocity (as shown in figure 13, where c_p denotes the particle number density and $\bar{c}_p$ represents its value averaged over the cross section). Air and particle velocity distributions under the same conditions as in figure 13 are shown in figure 14. The velocity profile

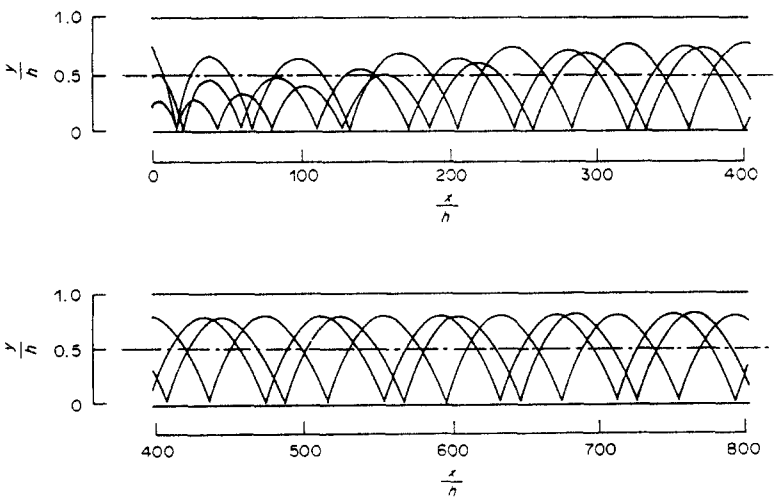

Figure 11. Particle trajectories ($\bar{u} = 15$ m/s, $\delta = 3\,\delta_0$).

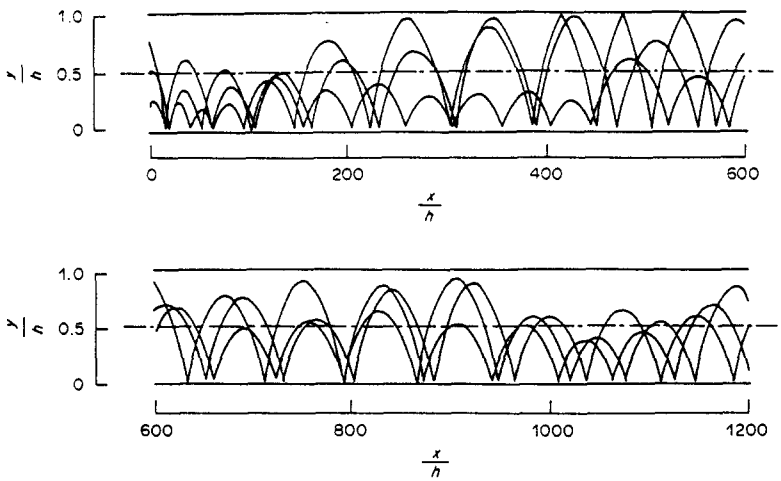

Figure 12. Particle trajectories ($\bar{u} = 15$ m/s, $\delta = 5\,R\delta_0$).

of air is flattened to some extent due to the particles but the profile is not as asymmetric as observed in the experiment. To remove this discrepancy, a power of R was considered and the coefficient δ given by

$$\delta = cR^k\delta_0. \qquad [15]$$

The above equation indicates that the probability of a small value of δ becomes higher if a large value is given to k. The physical interpretation of this is that the effect of abnormal bouncing is suppressed on average but some particles are allowed to jump extremely high. We found by trial and error that the following values for c and k give good agreement with measurements within the range of the present experiment:

$$c = 5, \quad k = 4. \qquad [16]$$

Calculations based on [16] are compared with measurements below. Figure 15 shows the particle concentrations at $\bar{u} = 7$ m/s and $\bar{u} = 15$ m/s. Agreement between calculations and measurements is satisfactory in the case of $\bar{u} = 7$ m/s, but not in the case of $\bar{u} = 15$ m/s. If the air velocity exceeds 15 m/s, the calculated concentration shows a uniform distribution.

Air and particle velocity distributions are shown in figures 16 and 17. In general, the air velocity profile in the horizontal flow becomes asymmetric at low air velocity and high loading ratio values. This tendency is greater in the measurements than the simulation. Figure 17 shows that the calculated particle velocities tend to be higher than the measured values.

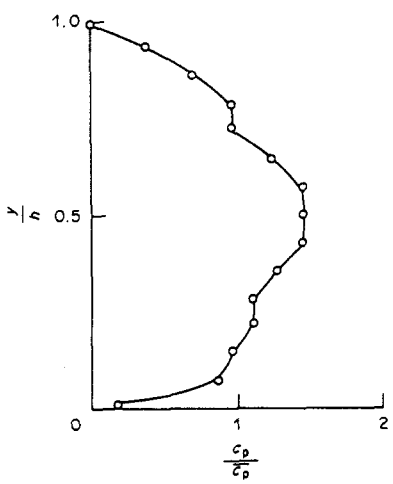

Figure 13. Particle concentration distribution ($\bar{u} =$ 7 m/s, $\delta = 5\,R\delta_0$).

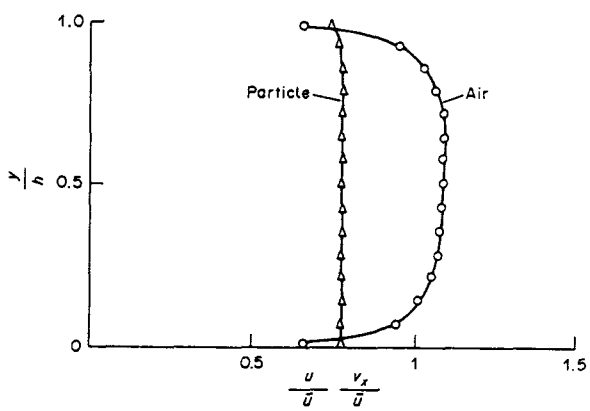

Figure 14. Air and particle velocity distributions ($\bar{u} =$ 7 m/s, $\delta = 5\,R\delta_0$).

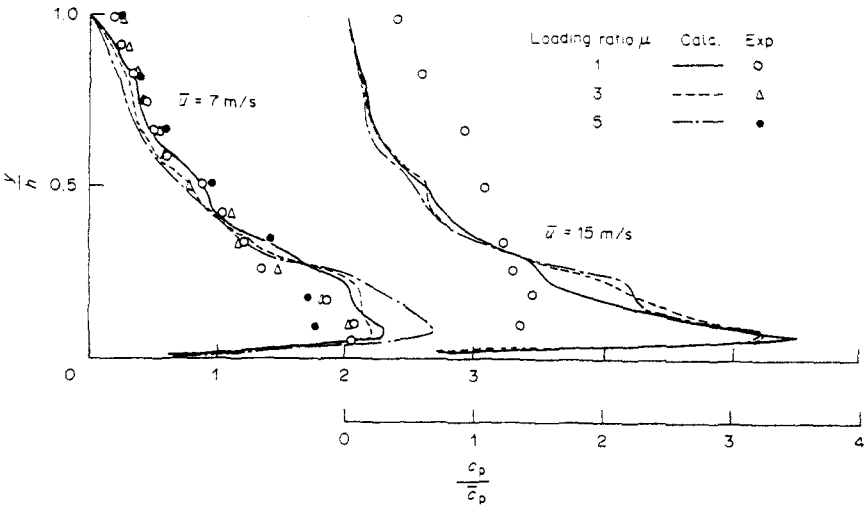

Figure 15. Particle concentration distribution ($\delta = 5R^4\delta_0$).

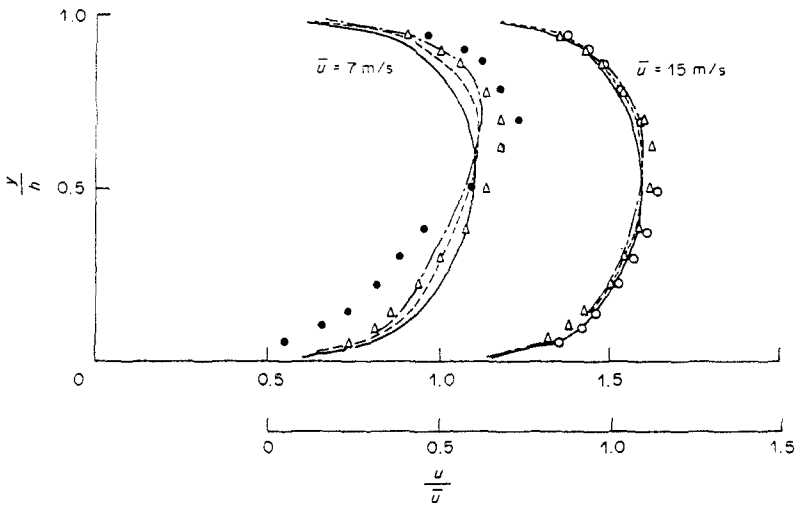

Figure 16. Air velocity distribution (for details see figure 15).

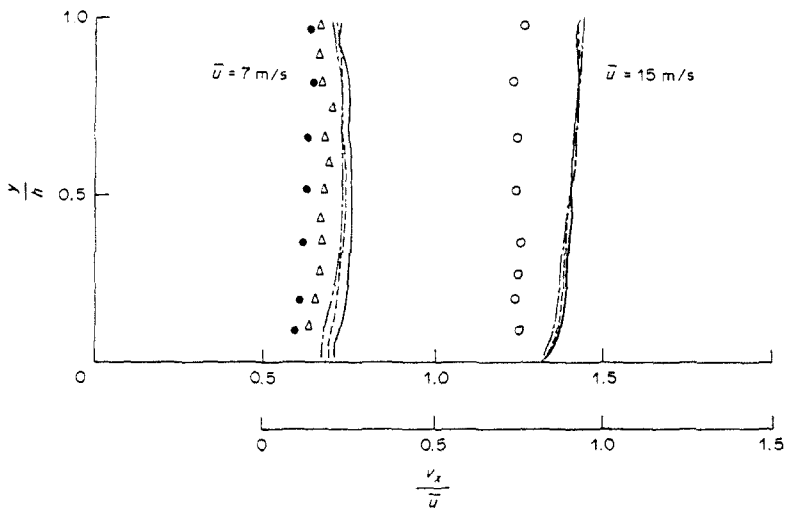

Figure 17. Particle velocity distribution (for details see figure 15).

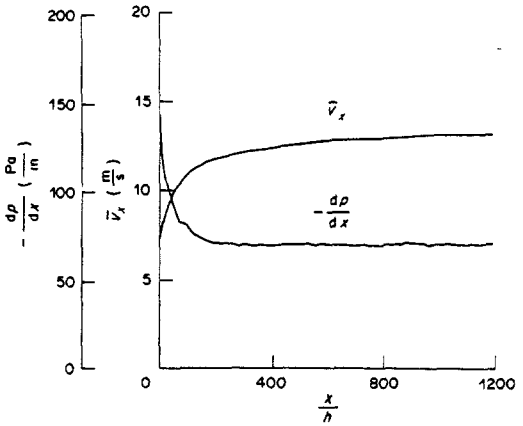

Figure 18. Particle velocity and pressure gradient variations ($\bar{u} = 15$ m/s, $\mu = 1$).

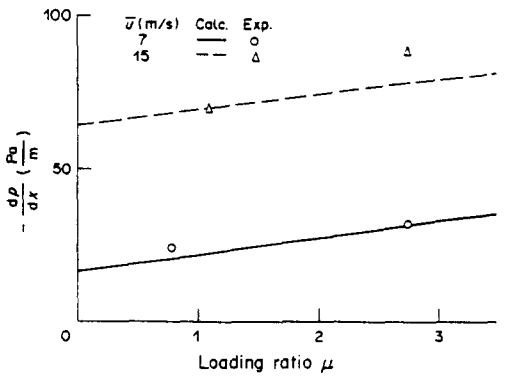

Figure 19. Relation between pressure gradient and loading ratio.

Figure 18 shows the calculated streamwise variations of the particle velocity $\bar{v}_x$ averaged over the cross section and the pressure gradient dp/dx. The pressure gradient measured in the region of fully-developed flow is compared with the calculated one in figure 19, the agreement is satisfactory.

5. DISCUSSION

A two-dimensional channel flow, which is seldom regarded as a practical means for particle transport, was chosen for this work because the treatment of equations of motion is simple. Owing to the simplicity of the field, a defect in the previous model for particle–wall collisions was found. Since the essence of the collision phenomenon does not change, whether in a two- or a three-dimensional field, the results obtained in the present work can be applied to pipe flows.

Tsuji *et al.* (1985) previously derived the model of abnormal bouncing, [12] and [13], from comparisons between calculations and measurements of pipe flow, where the particle size and pipe diameter changed, respectively, from 0.5 to 5 mm and from 27 to 200 mm. The effects of these dimensions have not been investigated in obtaining [15] and [16], which are presented for the first time in this work. Hence, it is necessary in the future to determine how such parameters affect the present empirical relations. If the empirical relations vary considerably according to the conditions, they are of little use as a model and alternative models must be sought.

Fluid turbulence is also a factor in the irregular motion of particles. Further, particle–particle collisions increase its importance as the concentration increases. Taking these factors into consideration in the model is a topic for future studies but improvement of the model should be made step by step, otherwise it is difficult to know which factor is dominant. The present work indicates, at least, that modeling of particle–wall collisions is a key factor in simulation of horizontal flows.

6. CONCLUSIONS

A numerical simulation was attempted to obtain the velocity profiles of air and solids, solid concentration and pressure drop in a two-dimensional channel. For the fluid phase, the boundary layer equation was solved using a finite-difference method developed by Patankar & Spalding (1970). For the solid phase, the Lagrangian method was used, with trajectories of many particle being calculated. It was found that the calculated results of particle concentration largely depend on the treatment of particle–wall collisions, particularly irregular bouncing. This irregular bouncing was taken into consideration by using a modified "virtual wall model" where the wall is replaced with a virtual one when the incident angle of a particle at the wall is less than a certain specified value. In addition to the simulation, an experiment was performed in a two-dimensional channel, where the particle and fluid motions were measured using a Pitot tube and an optical fiber probe. The experimental results were used to determine the empirical parameters in the bouncing model.

REFERENCES

CHEN, C. P. & WOOD, P. E. 1986 Turbulence closure modelling of the dilute gas–particle axisymmetric jet. *AIChE Jl* **32,** 163–166.

CROWE, C. T., SHARMA, M. P. & STOCK, D. E. 1977 The Particle-Source-In Cell (PSI.Cell) model for gas–droplet flows. *ASME Jl Fluid Engng* **99,** 325–332.

DENNIS, S. C. R., SINGH, S. N. & INGHAM, D. B. 1980 The steady flow due to a rotating sphere at low and moderate Reynolds numbers. *J. Fluid Mech.* **101,** 257–279.

DURST, F., MILOJEVIC, D. & SCHÖNUMG, B. 1984 Eulerian and Lagrangian predictions of particulate two-phase flows: a numerical study. *Appl. math. Modelling* **8,** 101–115.

MATSUMOTO, S., SAITO, S. & MAEDA, S. 1976 Simulation of gas–solid two-phase flow in a horizontal pipe. *J. chem. Engng Japan* **9,** 23–28.

MORIKAWA, Y., TSUJI, Y. & TANAKA, T. 1986 Measurements of horizontal air–solid two-phase flow using an optical fiber probe. *Bull. JSME* **29,** 802–809.

MOSTAFA, A. A. & ELGHOBASHI, S. E. 1985 A two-equation turbulance model for jet flows laden with vaporizing droplets. *Int. J. Multiphase Flow* **11,** 515–533.

PATANKAR, S. V. & SPALDING, D. B. 1970 *Heat and Mass Transfer in Boundary Layers.* Academic Press, New York.

SAFFMAN, P. G. 1965 The lift on a small sphere in a slow shear flow. *J. Fluid Mech.* **22,** 385–400.

SHUEN, J. S., SOLOMON, A. S. P., ZHANG, Q.-F. & FAETH, G. M. 1985 Structure of particle-laden jets: measurements and predictions. *AIAA Jl* **23,** 396–404.

TSUJI, Y. & MORIKAWA, Y. 1978 Computer simulation for the pneumatic transport in pipes with bends. *Proc. 4th Int. Conf. on the Pneumatic Transport of Solids in Pipes,* BHRA Fluid Engineering, Cranfield, U.K., Paper B1.

TSUJI, Y., SEKI, W. & MORIKAWA, Y. 1983 Computer simulation of pneumatic conveying: the case of the presence of pipe branches. *J. Soc. Powder Tech. Japan* **20,** 270–278 (in Japanese).

TSUJI, Y., OSHIMA, T. & MORIKAWA, Y. 1985 Numerical simulation of pneumatic conveying in a horizontal pipe. *KONA* **3,** 38–51.

APPENDIX

Collision Between a Single Particle and a Wall

Consider a three-dimensional collision of a spherical particle with a flat plate, as shown in figure A1. When the coefficients of restitution and kinetic friction are known, particle motions before and after the collision can be estimated by solving the impulsive equations. To solve the problem, the following assumptions are made:

(1) Plastic deformation and fracture are neglected.
(2) When the particle slides on the plate, the friction between the particle and plate obeys Coulomb's law.

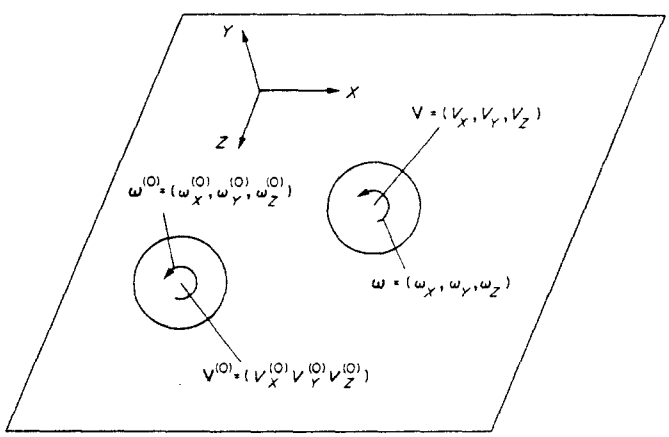

Figure A1. Collision of a spherical particle with a flat plate.

(3) Once the particle stops sliding it does not begin again.
(4) Throughout the collision process, the distance between the particle center of mass and the contact point is kept constant and equal to the particle radius a.

The process of collision is divided into two stages: the period during which the material in collision is compressed and the period during which this compression is released. The former and the latter are called the compression and recovery period, respectively. The coefficient of restitution e is defined by

$$e = \frac{J_n^{(2)}}{J_n^{(1)}}, \qquad [A.1]$$

where $J_n^{(1)}$ is the normal component of the impulse of the force which acts on a particle in the compression period and $J_n^{(2)}$ is the corresponding component in the recovery period. Coulomb's law states that the impulse of the friction force is the product of the impulse of the normal force and the coefficient of kinetic friction f. Thus, when the particle slides on the X–Z plane, the impulse $\mathbf{J}_t$ of the friction force is expressed as

$$\mathbf{J}_t = -\epsilon_X f \mathbf{J}_Y \mathbf{i} - \epsilon_Z f \mathbf{J}_Y \mathbf{k}, \qquad [A.2]$$

where $\mathbf{i}$ and $\mathbf{k}$ are unit vectors corresponding to the X- and Z-directions, and ϵ_X and ϵ_Z satisfy the following relation:

$$\epsilon_X^2 + \epsilon_Z^2 = 1. \qquad [A.3]$$

The signs of ϵ_X and ϵ_Z are defined to be identical to those of $V_X^{(0)} + a\omega_X^{(0)}$ and $V_X^{(0)} - a\omega_X^{(0)}$, respectively.

In general, particle collisions incorporate particle rotation. Thus $\mathbf{U}^{(0)}$, the velocity at the point at which the particle comes into contact with the wall, is the sum of the translation and rotation velocities, i.e.

$$\begin{aligned}\mathbf{U}^{(0)} &= \mathbf{V}^{(0)} + \mathbf{r} \times \omega \\ &= (V_X^{(0)} + a\omega_Z^{(0)})\mathbf{i} + V_Y^{(0)}\mathbf{j} + (V_Z^{(0)} - a\omega_X^{(0)})\mathbf{k}. \end{aligned} \qquad [A.4]$$

Before deriving the impulsive equations, one must note that there are three cases to consider regarding collision:

Case I: the particle stops sliding in the compression period.
Case II: the particle stops sliding in the recovery period.
Case III: the particle continues to slide throughout the collision.

For each of the above cases, the impulsive equations are derived by considering the momentum exchange.

Table A1 shows the velocities, angular velocities and impulses for each moment and period corresponding to Case I. The only known variables are $\mathbf{V}^{(0)}$ and $\omega^{(0)}$. The impulses $\mathbf{J}^{(s)}$, $\mathbf{J}^{(r)}$ and $\mathbf{J}^{(2)}$ are expressed as

$$\mathbf{J}^{(s)} = -\epsilon_X f \mathbf{J}^{(s)}\mathbf{i} + \mathbf{J}_Y^{(s)}\mathbf{j} - \epsilon_Z f \mathbf{J}_Y^{(s)}\mathbf{k}, \qquad [A.5]$$

$$\mathbf{J}^{(r)} = \mathbf{j}_X^{(r)}\mathbf{i} + \mathbf{J}_Y^{(r)}\mathbf{j} + \mathbf{J}_Z^{(r)}\mathbf{k} \qquad [A.6]$$

Table A1. Collision parameters for Case I

(0) Before the collision	(1) Compression period		(2) Recovery period	After the collision
	← The particle slides →			
	(s)	(r)		
Velocity	$\mathbf{V}^{(0)}$	$\mathbf{V}^{(s)}$	$\hat{\mathbf{V}}$	$\mathbf{V}$
Angular velocity	$\omega^{(0)}$	$\omega^{(s)}$	$\hat{\omega}$	ω
Impulse		$\mathbf{J}^{(s)}$	$\mathbf{J}^{(r)}$	$\mathbf{J}^{(2)}$

and

$$\mathbf{J}^{(2)} = \mathbf{J}_X^{(2)}\mathbf{i} + e(\mathbf{J}_Y^{(s)} + \mathbf{J}_Y^{(r)})\mathbf{j} + \mathbf{J}^{(2)}\mathbf{k}. \quad [A.7]$$

Considering the momentum exchange at each moment, one has the following impulsive equations:

$$M(\mathbf{V}^{(s)} - \mathbf{V}^{(0)}) = \mathbf{J}^{(s)}, \quad [A.8]$$

$$M(\hat{\mathbf{V}} - \mathbf{V}^{(s)}) = \mathbf{J}^{(r)}, \quad [A.9]$$

$$M(\mathbf{V} - \hat{\mathbf{V}}) = \mathbf{J}^{(2)}, \quad [A.10]$$

$$I(\omega^{(s)} - \omega^{(0)}) = -\mathbf{r} \times \mathbf{J}^{(s)}, \quad [A.11]$$

$$I(\hat{\omega} - \omega^{(s)}) = -\mathbf{r} \times \mathbf{J}^{(r)} \quad [A.12]$$

and

$$I(\omega - \hat{\omega}) = -\mathbf{r} \times \mathbf{J}^{(2)}, \quad [A.13]$$

where M and I are the particle mass and moment of inertia, respectively.

The boundary conditions are

$$[\mathbf{V}^{(s)} + \mathbf{r} \times \omega^{(s)}]_t = 0, \quad [A.14]$$

$$\hat{\mathbf{V}} + \mathbf{r} \times \hat{\omega} = 0 \quad [A.15]$$

and

$$[\mathbf{V} + \mathbf{r} \times \omega]_t = 0, \quad [A.16]$$

where the subscript t denotes the tangential component.

The solutions to Case I are shown in column (1) of table A1; the solutions to Cases II and III, which are the same, are shown in column (2).